ELSEVIER

Chemical Engineering Journal 129 (2007) 41–49

Chemical Engineering Journal

www.elsevier.com/locate/cej

A kinetic study of the combustion of porous synthetic soot

R. López-Fonseca, I. Landa, U. Elizundia, M.A. Gutiérrez-Ortiz, J.R. González-Velasco *

Chemical Technologies for Environmental Sustainability Group, Department of Chemical Engineering, Faculty of Science and Technology, Universidad del País Vasco/EHU, P.O. Box 644, E-48080 Bilbao, Spain

Received 16 May 2006; received in revised form 30 October 2006; accepted 31 October 2006

Abstract

This work confirms the utility of a composite kinetic processing technique based on the complementary use of both isoconversional method and master-plot methods in ascribing the kinetic triplet (conversion model, pre-exponential factor and activation energy) of monitored nonisothermal combustion of synthetic porous soot in air by thermogravimetry at different heating rates. Firstly, the activation energy value was obtained (153 kJ mol^{-1}) from the Kissinger–Akahira–Sunose isoconversional method. Secondly, the appropriate conversion model of the process was selected by means of the master-plot method. The combustion of the soot was found to follow a mechanism based on surface nucleation with subsequent movement of the resulting surface, which was consistent with the penetration of oxygen through the porous structure of the solid sample. Comparing both experimental and calculated thermoanalytical curves at constant heating rate assessed the adequate consistency of the kinetic triplet. Further, the combustion process was isothermally simulated.

Keywords: Soot; Combustion kinetics; Thermal analysis; Isoconversional methods; Master-plot method

1. Introduction

Kinetic analysis of solid-state reactions is most frequently undertaken to obtain a mathematical representation of reaction data. The search for a mathematical description of experimental data is usually sought in terms of a kinetic triplet (Arrhenius parameters A and E_a, and the reaction model). A number of heterogeneous solid–gas thermo-oxidative reactions, such as the degradation of polymeric materials [1,2], can be kinetically evaluated by means of thermoanalytical methods (mainly, thermogravimetry, differential thermal analysis, and differential scanning calorimetry), which measure an extensive property of a system [3]. This study states our approach to the development of kinetic expressions of another example of this type of reactions, the combustion of carbonaceous particulate matter. A wide range of calculation techniques has been proposed for deriving the kinetic triplet from thermoanalytical kinetic data. These methods can be classified according to the experimental conditions selected (isothermal or nonisothermal conditions) and the mathematical analysis performed (model-fitting and isoconversional model-free methods) [4].

The aim of this work is specifically to show the utility of a composite kinetic analysis method based on the complementary use of both isoconversional and master-plot methods from nonisothermal thermogravimetric data in selecting the most accurate kinetic triplet of the combustion of a porous carbon black selected as a diesel particulate surrogate (synthetic soot). Obtained parameters may be useful for a number of practical applications; for example, modelling the regeneration of the trap in diesel-powered vehicles, determining the efficiency of a given catalyst for lowering the soot combustion temperature, comparison between reaction kinetics and properties of the solid, and a better understanding of the physico-chemical properties (composition, amount of adsorbed hydrocarbons, surface area, crystallographic structure) of different carbonaceous materials [5–7]. Note that since it is difficult to obtain diesel soot with constant properties (the composition depends on many engine characteristics such as engine load, speed, fuel, and in-cylinder temperature) a commercially available model soot (produced by Aldrich) was used for reproducibility reasons.

1.1. Rate laws and kinetic analysis

Kinetic studies of thermally stimulated reactions in solids are frequently performed under isothermal or nonisothermal conditions. Eq. (1) is used to describe the kinetics of these reactions

* Corresponding author. Tel.: +34 94 6012681; fax: +34 94 6015963.
E-mail address: juanra.gonzalezvelasco@ehu.es (J.R. González-Velasco).

1385-8947/$ – see front matter © 2006 Elsevier B.V. All rights reserved.
doi:10.1016/j.cej.2006.10.029

Table 1
List of reaction models commonly used to represent solid-state reaction kinetics

Reaction model	Symbol	Differential kinetic function $f(\alpha)$	Integral kinetic function $g(\alpha)$
Nucleation and growth (Avrami–Erofeev equation)	$A_{1.5}$	$1.5(1-\alpha)(-\ln(1-\alpha))^{1/1.5}$	$(-\ln(1-\alpha))^{1/1.5}$
Nucleation and growth (Avrami–Erofeev equation)	A_2	$2(1-\alpha)(-\ln(1-\alpha))^{1/2}$	$(-\ln(1-x))^{1/2}$
Nucleation and growth (Avrami–Erofeev equation)	A_3	$3(1-\alpha)(-\ln(1-\alpha))^{1/3}$	$(-\ln(1-\alpha))^{1/3}$
Nucleation and growth (Avrami–Erofeev equation)	A_4	$4(1-\alpha)(-\ln(1-\alpha))^{1/4}$	$(-\ln(1-\alpha))^{1/4}$
Phase boundary controlled reaction (contracting linear)	P_1	1	α
Phase boundary controlled reaction (contracting area)	P_2	$3(1-\alpha)^{2/3}$	$(1-(1-\alpha)^{1/2})$
Phase boundary controlled reaction (contracting volume)	P_3	$2(1-\alpha)^{1/3}$	$(1-(1-\alpha)^{1/3})$
One-dimensional diffusion	D_1	$(1/2)\alpha^{-1}$	α^2
Two-dimensional diffusion	D_2	$[-\ln(1-\alpha)]^{-1}$	$(1-\alpha)\ln(1-\alpha)+\alpha$
Three-dimensional diffusion	D_3	$2(1-\alpha)^{2/3}(1-(1-\alpha)^{1/3})^{-1}$	$(1-(1-\alpha)^{1/3})^2$
Ginstling–Brounshtein equation	D_4	$(2/3)(1-\alpha)^{1/3}[1-(1-\alpha)^{1/3}]^{-1}$	$(1-2/3\alpha)-(1-\alpha)^{2/3}$
Chemical reaction (first order)	R_1, A_1	$1-\alpha$	$(-\ln(1-\alpha))$
Chemical reaction (second order)	R_2	$(1-\alpha)^2$	$(1-\alpha)^{-1}-1$
Power law I	L_1	$4\alpha^{3/4}$	$\alpha^{1/4}$
Power law II	L_2	$3\alpha^{2/3}$	$\alpha^{1/3}$
Power law III	L_3	$2\alpha^{1/2}$	$\alpha^{1/2}$
Power law IV	L_4	$2/3\alpha^{-1/2}$	$\alpha^{3/2}$
Zhuravlev equation	D_5	$(2/3)(1-\alpha)^{5/3}[1-(1-\alpha)^{1/3}]^{-1}$	$[(1-\alpha)^{-1/3}-1]^2$

under linear heating, where $f(\alpha)$ is the reaction model (Table 1), also called the conversion function, α the extent of conversion, $k(T)$ the Arrhenius rate constant, T the absolute temperature, β the constant heating rate, A the pre-exponential factor, and E_a is the activation energy:

$$\frac{d\alpha}{dT} = \frac{A}{\beta} e^{-E_a/RT} f(\alpha) \quad (1)$$

Upon integration Eq. (1) gives

$$g(\alpha) = \frac{A}{\beta}\int_{T_0}^{T} e^{-E_a/RT}\,dT = \frac{AE_a}{\beta R}\int_x^{\infty}\frac{e^{-x}}{x^2}\,dx = \frac{AE_a}{\beta R}p(x) \quad (2)$$

where $g(\alpha)$ is the integral degradation model, $x = E_a/RT$, and $p(x)$ is the exponential integral, which has no analytical solution. To overcome this difficulty, the exponential integral has been solved using approximation methods, series expansions, and numerical solution methods [8].

Kinetic parameters can be obtained by both model-fitting and isoconversional methods. For nonisothermal experiments, model-fitting involves fitting different models to α–T curves and simultaneously determining E_a and A. There are numerous nonisothermal model-fitting methods; one of the most popular is the Coats–Redfern (CR) method [9], which is formalised by Eq. (3). Thus, the model that gives the best linear-fit is usually selected as the model of choice:

$$\ln\frac{g(\alpha)}{T^2} = \ln\left(\frac{AR}{\beta E_a}\left[1-\frac{2RT}{E_a}\right]\right) - \frac{E_a}{RT} \quad (3)$$

Nevertheless, the use of model-fitting (modelistic) methods has been criticised in nonisothermal studies because regression methods may lead to indistinguishable fits or mathematical expressions with high correlation [10,11]. As a result, the values of the Arrhenius parameters, obtained for various forms of $g(\alpha)$, are correlated through the relation of compensation effect [12,13].

In contrast, isoconversional methods, which allow for model-independent estimates of the activation energy at progressive degrees of conversion by conducting multiple experiments at differing constant heating rates, are highly recommended in order to obtain a reliable kinetic description [14]. The attractiveness of the isoconversional methods is that A and $g(\alpha)$, which are assumed to remain unchanged, are unneeded for the calculation of E_a. Thus, substituting $p(x) = \exp(-x)/x^2$ as an approximate expression in Eq. (2) [4], Eq. (4) is obtained, which is the basis of the model-free isoconversional method developed by Kissinger, Akahira and Sunose (KAS method) [15]:

$$\ln\frac{\beta}{T^2} = \ln\left[\frac{AE_a}{Rg(\alpha)}\right] - \frac{E_a}{RT} \quad (4)$$

The physico-chemical conversion model ($f(\alpha)$ or $g(\alpha)$) of solid-state reactions can be determined by using the so-called master-plot method. Master plots are reference theoretical curves depending on the kinetic model but generally independent of the kinetic parameters of the process [16]. Essentially the master-plot method is based on the comparison of theoretical master plots, which are obtained for a wide range of ideal kinetic models, with the experimental master plot. This comparison obviously requires the previous transformation of the experimental data into the corresponding master plot. The application of this method usually leads to the selection of the appropriate conversion model for the solid-sate reaction investigated [17]. Mathematically the use of this master-plot method for kinetic data recorded under nonisothermal conditions is describes as follows.

By using a reference at point $\alpha = 0.5$ and according to Eq. (2), the following equation is obtained:

$$g(0.5) = \frac{AE_a}{\beta R}p(x_{0.5}) \quad (5)$$

where $x_{0.5} = E/RT_{0.5}$, and $T_{0.5}$ is the temperature required to attain 50% conversion. When Eq. (2) is divided by Eq. (5), Eq. (6)

is deduced:

$$\frac{g(\alpha)}{g(0.5)} = \frac{p(x)}{p(x_{0.5})} \quad (6)$$

Plotting $g(\alpha)/g(0.5)$ versus α corresponds to theoretical master plots of various $g(\alpha)$ functions. Both the conversion–temperature profile (α–T) and the value of E_a for the process should be known in advance in order to draw the experimental master plots of $p(x)/p(x_{0.5})$ versus α from experimental data obtained at a given heating rate. Thus, Eq. (6) indicates that, for a given α, the experimental value of $p(x)/p(x_{0.5})$ and theoretically calculated values of $g(\alpha)/g(0.5)$ are equivalent when an appropriate conversion model is used.

1.2. Thermo-kinetic curves reconstruction and stability prediction

It is of importance to reliably predict the thermal stability of the material in extended temperature ranges (these difficulties are prevalent at low temperatures, requiring very long scanning time) and also under temperature conditions at which the investigation of the properties is very difficult to achieve or simply has not been carried out (for example, at other heating rates).

The knowledge of the apparent E_a value is sufficient to extrapolate the isothermal kinetics from nonisothermal data. This is described by Eq. (7):

$$t_\alpha = \frac{\int_0^{T_\alpha} e^{-E_a/RT}\,dT}{\beta\, e^{-E_a/RT_0}} \quad (7)$$

where T_α is an experimental value of the temperature corresponding to a given conversion at the heating rate β. This equation enables the time (t_α) at which a given conversion will be reached at an arbitrary temperature, T_0, to be computed. Solving Eq. (7) for different conversions the dependence of α on t at a given temperature can be predicted [18].

The kinetic behaviour of the solid can be also simulated to other heating rates that were not used in the kinetic analysis. By virtue of the assumption that the mechanism remains unchanged, the quantities $g(\alpha)$ will be the same for equal transformation degrees at different heating rates. Therefore, the following equation can be deduced:

$$\frac{p(x)_{T_x}}{\beta_x} - \frac{p(x)_{T_0}}{\beta_0} = 0 \quad (8)$$

A numerical solution of Eq. (8) makes it possible, at a given heating rate β_x, to find the temperature T_x corresponding to the transformation degree that was reached in the nonisothermal experiment (at the heating rate β_0) at temperature T_0 [19].

The algorithms presented for calculating the dependences α on t with T = constant and α on T with β = constant are based on the assumption that the Arrhenius parameters do not change when the heating rate varies. Moreover, the absence of both the kinetic model and the pre-exponential factor in predictive equations means that these components do not include corresponding errors when making kinetic predictions. Thus, provided that the assumptions made above are valid, these two components of the kinetic triplet are not necessary in extrapolating experimental results to other set of conditions.

2. Experimental

The carbon soot (390127-25G) was obtained from Aldrich, and was used as received. This material is made up of individual, basically spherical carbon particles of about 20 nm. The carbon, hydrogen and nitrogen content of the samples was determined in an automatic Leco CHN-2000 equipment, the sulfur content was established using an automatic Leco S-144-DR apparatus, and the oxygen content was measured by means of a Leco VTF-900 pyrolytic furnace connected to a Leco CHNS-932 microanalyser. The content of volatile adsorbed species (water and hydrocarbons) was measured by temperature-programmed desorption in N_2 up to 873 K at a heating rate of 1.5 K min^{-1}. The ash content was determined by combustion at 1273 K in a muffle furnace. The textural properties were determined by N_2 adsorption–desorption at 77 K in a Micromeritics ASAP 2010 equipment in a relative pressure range from about 10^{-6} to 0.99. The sample was previously evacuated overnight at 423 K under high vacuum. The BET area (S_{BET}) was obtained fitting this model to the adsorption isotherm in the N_2 relative pressure range of 0.002–0.3.

The thermo-oxidative degradation of the carbonaceous materials was investigated by means of dynamic thermogravimetry using a Perkin-Elmer TGS-2 thermobalance under atmospheric pressure. The mass loss and the sample temperature were continuously recorded by a computerised data acquisition system. The studies were carried out at constant heating rates of 1.5, 3.0, 5.0, and 7.5 K min^{-1}. The oxidant stream was dry air (50 cm^3 min^{-1}) flowing downwards onto the cylindrical sample holder. The samples for thermogravimetric analysis were prepared by simply mixing the corresponding carbonaceous material and silicon carbide (SiC) with a spatula in a mass ratio of 1/10. The addition of SiC decreased the flow resistance of the sample bed and provided a heat sink, which decreased temperature gradients in the sample. Employing sample sizes of 0.5 g carbonaceous material diluted with about 5 g SiC, thermal runaways as well as strong heat-up of the samples during thermogravimetric analyses were avoided. Thus, the sample for each run was 25 mg of the mixture (around 2.3 mg of carbonaceous material). The experimental conditions such as sample size, dilution ratio, atmosphere and gas flow rate were identical in all kinetic experiments. Since dry air feed was supplied in large excess the combustion reaction took place with a negligible oxygen partial pressure change. Therefore, the effect of the oxygen partial pressure on the process could be considered constant.

3. Results and discussion

On a dry basis, the synthetic soot had a carbon content of 97.4 wt.%, a hydrogen content of 0.4 wt.%, a nitrogen content of 0.7 wt.%, an oxygen content of 0.8 wt.%, and a sulfur content of 0.8 wt.%. The lack of inorganic elements ensured the absence of catalytic effects on the combustion process. The moisture content was relatively low (1.8 wt.%). The sample

contained approximately 10 wt.% of adsorbed hydrocarbons, as revealed by temperature-programmed desorption in nitrogen up to 600 °C. The BET surface area of the carbon soot determined by N_2 adsorption at 77 K amounted approximately 80 $m^2\ g^{-1}$. It could be observed that the isotherm of nitrogen for the carbon soot was typical of a mesoporous solid. The hysteresis loop shape was that found for slit-shaped pores according to the classification by IUPAC [20].

Prior to the kinetic analysis, the effects of heat- and mass-transfer limitations on the results of thermoanalytical measurements were eliminated. For exothermal reactions, the heat-transfer limitations could be minimised by diluting the carbonaceous sample with an excess of an inert material. Silicon carbide has been reported to be a suitable inert material with a high heat capacity and a high thermal conductivity [21]. The addition of SiC also facilitated the transfer of oxidant within the bed due to its larger particle size (37–74 μm) in comparison with that of the sample, thereby reducing oxygen concentration gradients. In this sense, it was preferable that the rate of mass-transfer was high enough to maintain the oxygen concentration at the surface of the bed at the bulk level. Obviously, a downward flow was desirable with the lip of the crucible as short as possible. Thus, a series of exploratory experiments was performed with varying dilution mass ratio (1/20, 1/10, and 1/5), sample size (10, 25, and 35 mg), and gas flow rate of dry air (25, 50, 100, and 200 $cm^3\ min^{-1}$) in order to define the window where heat- and mass-transfer limitations could occur. All these experiments were conducted at a constant heating rate of 3 K min^{-1}. It was observed that irrespective of the experimental conditions the conversion versus temperature curves remained unaffected within the range of experimental uncertainty. Moreover, assuming an effective diffusion coefficient within the bed of 0.05 $cm^2\ g^{-1}$ [22] and a bed depth of 1.8 mm, a bed Thiele modulus ranging from 0.1 to 0.2 was obtained. This meant that the assumption of complete oxygen penetration was justified [23]. On the other hand, the results calculated for the Thiele modulus applied to reaction within an individual particle [24] were less than 0.01 for all temperatures. Hence, a flow rate of dry air of 50 $cm^3\ min^{-1}$, a dilution mass ratio of 1/10, and a sample size of 25 mg (2.3 mg of carbonaceous material and 22.7 mg of SiC) were selected as experimental conditions for kinetic experiments.

3.1. Determination of the activation energy by KAS isoconversional method

The conversion–temperature curves recorded at 1.5, 3, 5 and 7.5 K min^{-1} are shown in Fig. 1. These sigmoidal-shaped curves showed a noticeable dependence of the conversion degree attained at a given temperature on the heating rate in such a way that they were shifted to higher temperatures at higher heating rates. Note that the symmetry was slightly distorted at low conversion degrees. In fact, the curves practically overlapped in the 0–0.1 conversion range. This phenomenon was likely to be explained by the presence of reactive hydrocarbons, which were easily oxidised irrespective of the heating rate employed [25].

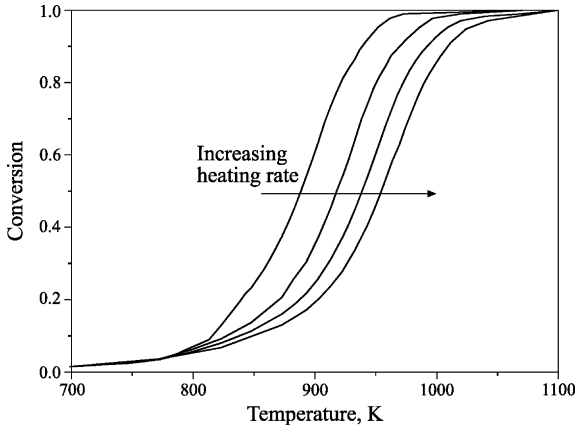

Fig. 1. Experimental mass kinetic curves obtained at different heating rates (1.5, 3, 5 and 7.5 K min^{-1}).

The KAS isoconversional method essentially involves measuring the temperatures corresponding to fixed values of α from experiments at different heating rates. It is widely accepted that there is always the possibility of deviation of experimental data from theoretical values at the extremities of reaction. Therefore, special consideration was given to the influence of limiting data (at both low (<0.1) and high (>0.9) α values) on the calculation of the regression line and criteria used to measure excellence of fit [26]. In this study, this contribution mainly resulted from the fast decomposition of adsorbed hydrocarbons (impurities) in the solid reactant. Unless recognised and separated, this initial deviation would lead to a less precise fit. Hence, the kinetic analysis was focused on the dominant reaction alone (0.1–0.9 conversion range). When plotting $\ln(\beta/T^2)$ versus $1/T$ at the same degree of conversion, a family of straight ($r^2 > 0.99$), nearly parallel lines was obtained (Fig. 2). Thus, the activation energy for a certain extent of conversion could be obtained from the slope of such lines. It was evidenced that the activation energy hardly varied with the extent of conversion (single-step reaction). Hence, a mean value of 153 kJ mol^{-1} was calculated, and reported as the apparent activation energy of the process. Excluding highly heat-treated carbon, there is relative agreement about the magni-

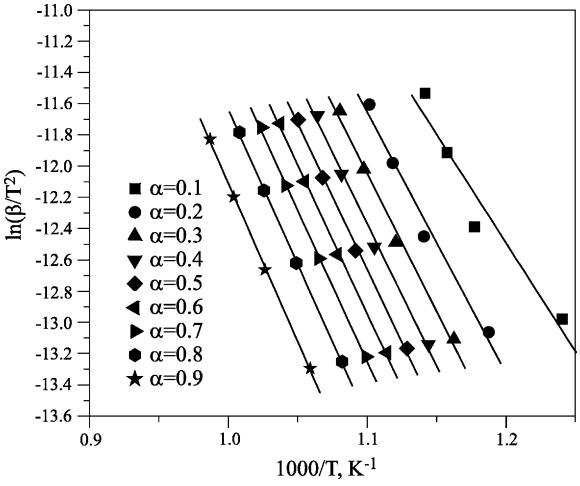

Fig. 2. Isoconversional (KAS method) plots at various conversion degrees.

Table 2
Results from the application of the CR method (Eq. (3)) for various kinetic models

Model	$\beta = 1.5$ K min^{-1}			$\beta = 3$ K min^{-1}			$\beta = 5$ K min^{-1}			$\beta = 7.5$ K min^{-1}		
	E (kJ mol^{-1})	ln A[a] (min^{-1})	r^2	E (kJ mol^{-1})	ln A[a] (min^{-1})	r^2	E (kJ mol^{-1})	ln A[a] (min^{-1})	r^2	E (kJ mol^{-1})	ln A[a] (min^{-1})	r^2
$A_{1.5}$	83	7.74	0.99	81	7.59	0.97	82	8.10	0.97	85	8.71	0.99
A_2	56	3.84	0.99	55	3.93	0.97	56	4.45	0.97	58	4.96	0.98
A_3	30	−0.21	0.99	30	0.03	0.96	30	0.55	0.96	31	1.03	0.97
A_4	18	−2.74	0.94	17	−2.08	0.94	17	−1.65	0.94	18	−1.18	0.96
P_1	88	12.19	0.99	88	12.88	0.99	88	13.39	0.99	90	8.91	0.99
P_2	109	9.55	0.99	108	10.23	0.99	108	10.75	0.99	112	11.33	0.99
P_3	117	10.31	0.99	115	10.99	0.99	116	11.51	0.99	120	12.09	0.99
D_1	197	21.24	0.99	197	21.93	0.99	197	22.44	0.99	203	23.15	0.99
D_2	222	24.16	1.00	221	24.85	1.00	222	25.37	1.00	229	26.10	1.00
D_3	254	27.23	0.99	252	27.92	0.99	255	28.44	0.99	262	29.21	0.99
D_4	233	25.97	0.99	231	24.85	0.99	233	25.37	0.99	240	26.12	0.99
R_1, A_1	134	15.04	1.00	132	14.85	0.98	134	16.40	0.98	138	15.74	0.99
R_2	198	24.68	0.97	195	24.08	0.94	199	24.42	0.94	204	25.05	0.95
L_1	6	−5.19	0.69	6	−4.73	0.79	6	−4.22	0.97	6	−3.86	0.81
L_2	15	−3.11	0.89	15	−2.65	0.94	15	−2.28	0.94	15	−1.81	0.94
L_3	33	0.01	0.95	33	0.40	0.97	33	0.74	0.97	34	1.22	0.97
L_4	143	15.50	0.97	142	15.40	0.99	142	15.48	0.99	147	16.11	0.99
D_5	254	29.16	0.99	252	28.38	0.99	255	28.44	0.99	262	29.21	0.99

[a] A in min^{-1}.

tude of the activation energy for the combustion of carbonaceous materials; it falls between 105 and 180 kJ mol^{-1} with many values in the range 130 to 160 kJ mol^{-1} [27–33]. The variation in these values is generally attributed to surface heterogeneity and structural properties of different types of carbons.

As for real soot samples it should be noted that their properties notably differ from those of synthetic soot. Normally, they contain a greater fraction of adsorbed hydrocarbons and the carbonaceous matrix is usually more reactive. Hence, the combustion process generally occurs according to a two-step scheme. Firstly, adsorbed hydrocarbons are oxidised at relatively low temperatures (about 350–400 °C) while the combustion of the solid part takes place at temperatures higher than 550 °C. It is believed that the use of isoconversional methods can be appropriate for studying the kinetics of each process [34].

Table 2 shows the results of the application of the Coats–Redfern method for various kinetic models to the experimental kinetic data recorded at 1.5, 3, 5 and 7.5 K min^{-1} in terms of E_a, ln A and r^2. It was found that the values of the Arrhenius parameters depended on the kinetic model (strong dependence) as well on the heating rate (weak dependence). The high (>0.97) r^2 value obtained by a large number of conversion models did not permit an unambiguous choice of the conversion model of the process. It was noted that any thermogravimetric curve could be apparently described by various kinetic models as a consequence of the mutual correlation of the kinetic parameters E_a and A [35]. It is therefore evident that this method as a unique strategy for kinetic calculations should be avoided.

3.2. Determination of the conversion model

Fig. 3 shows the theoretical master plots corresponding to the $g(\alpha)$ functions listed in Table 1. The master plots coincide with $g(\alpha)/g(0.5) = 0$ at $\alpha = 0$ and $g(\alpha)/g(0.5) = 1$ at $\alpha = 0.5$, but reasonable large differences among different $g(\alpha)$ functions assumed are apparent within the range $\alpha > 0.5$. As said previously, the knowledge of α as a function of temperature and the value of the activation energy are essential in order to calculate the experimental master plot of $p(x)/p(x_{0.5})$ against α from experimental data obtained under a linear heating rate (Eq. (6)). Fig. 4 includes the experimental master plots of $p(x)/p(x_{0.5})$ versus α constructed from experimental data under a heating rate of 5 K min^{-1}. Although not shown, it was noticed that all experimental master plots closely matched each other irrespective of the heating rate. The comparison of the experimental master plots with theoretical ones revealed that the kinetic process for the combustion of the model carbon was most probably described by the A_m (Avrami–Erofeev) model, $g(\alpha) = (-\ln(1-\alpha))^{1/m}$ with the m value close to the unity (Fig. 4). However, the occurrence of a conversion model based on a shrinking-core model (P_3), which is typically assigned as the governing conversion model in the combustion of a variety of carbonaceous materials [36,37], could not be ruled out due to the close proximity over the 0.1–0.75 conversion range.

An attempt was made to relate the computational results to the actual sequence of physico-chemical processes occurring with the aid of complementary information from ex situ textural analysis of partially converted samples. Thus, a series of samples decomposed to conversion degrees ranging from 30% to 80% were prepared, and subsequently analysed by N_2 adsorption–desorption at 77 K. Remarkable changes in surface areas due to mass removal were noted [38,39]. Fig. 5 reveals that the BET surface area rapidly increased with conversion, and at about 60% conversion reached a maximum value of 500 m^2 g^{-1}, that was as much as six times the area before combustion. The surface area of all partially converted samples was remarkably greater than that obtained if a shrinking-core model were applied to the spherules. Consequently, an internal development of porosity was responsible for the notable increase in surface area as the combustion proceeded [25,40].

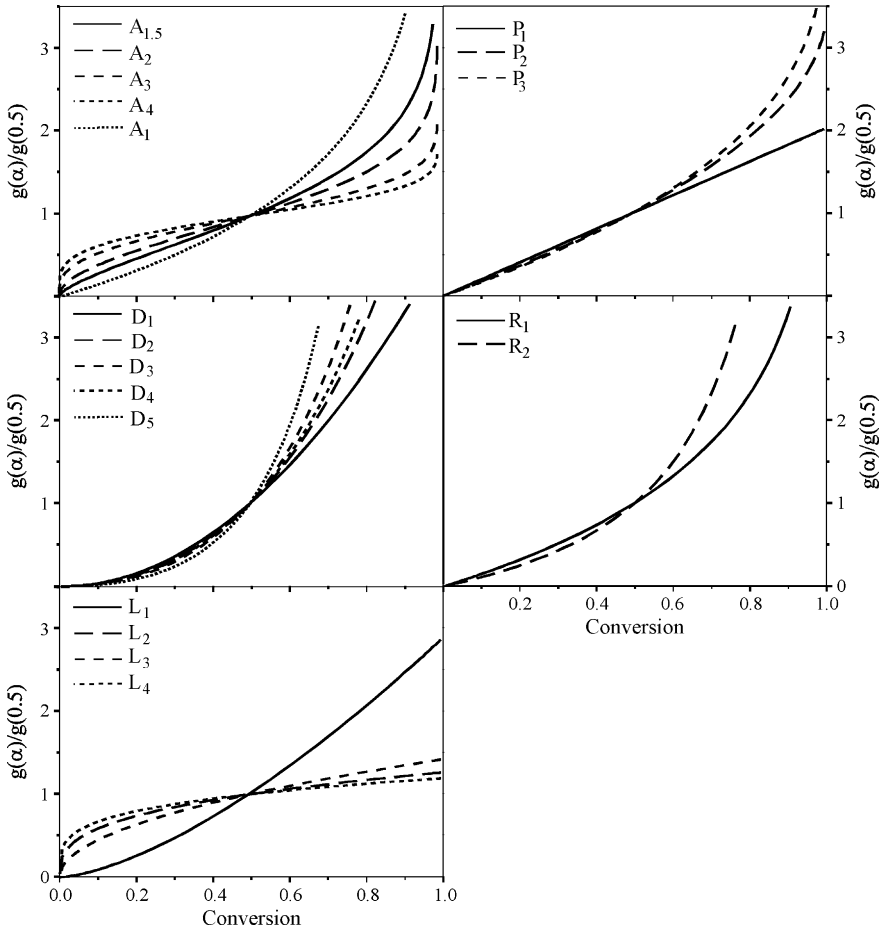

Fig. 3. Master plots of theoretical $g(\alpha)/g(0.5)$ vs. α for the conversion models listed in Table 1.

3.3. Determination of the pre-exponential factor

If the conversion model of the combustion of the synthetic soot were considered to obey an A_m model, it would be, however, likely that the reaction geometry of the overall reaction could not be expressed in terms of an integral value of m. In fact, a nonintegral exponent was introduced because it was expected that the idealised conditions for nucleation and nuclei growth could not be met in the reaction process. It must be indicated that any of the conversion function included in Table 1 has been derived by considering ideal models (homogeneous particle size, shape, etc.), conditions that are not always satisfied by commercial samples.

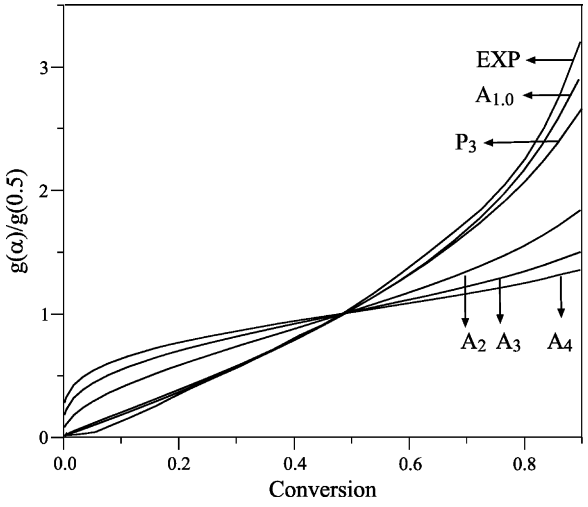

Fig. 4. Master plots of theoretical $g(\alpha)/g(0.5)$ vs. α for various conversion models and experimental master plot (EXP curve) for the combustion process at a heating rate of 5 K min^{-1}.

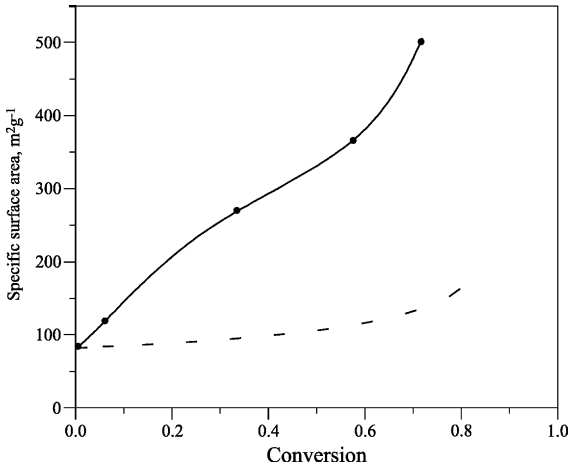

Fig. 5. Evolution of BET surface area with burn-off (solid line, experimental data; dashed line, evolution according to the shrinking-core model).

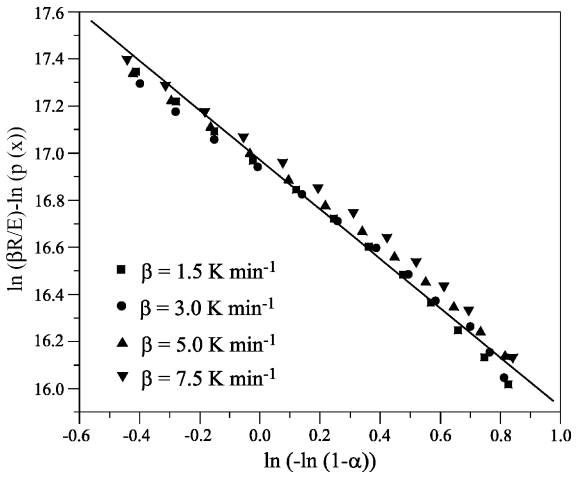

Fig. 6. $\ln[\beta R/E] - \ln[p(x)]$ vs. $\ln[-\ln(1-\alpha)]$ plots for the combustion of model soot at several heating rates and its linear-fit drawing.

Thus, the most appropriate conversion model was estimated as the A_m function with noninteger kinetic exponent m, which was used to accommodate the distortion between the actual and idealised nucleation and nuclei growth models. By assuming the A_m law, experimental data, the expression for the A_m model, and the average activation energy predetermined were then introduced into Eq. (2) and, as a result the following expression was deduced (Eq. (9)):

$$\ln \frac{\beta R}{E} - \ln\ p(x) = \ln\ A - \frac{1}{m} \ln[-\ln(1-\alpha)] \quad (9)$$

A set of lines was obtained by plotting $\ln(\beta R/E) - \ln(p(x))$ versus $\ln(-\ln(1-\alpha))$. As shown in Fig. 6, the lines corresponding to various heating rates superposed each other nearly completely. This verified the negligible dependence of the conversion model on the heating rate. The resulting logarithmic values of the pre-exponential factor and the kinetic exponent m are listed in Table 3. It was observed that a change in the heating rate induced no remarkable change in the values of $\ln A$ and m exponent, which was consistent with a common single-step reaction [18]. It could be therefore concluded that the possible mechanism for the combustion of the selected material was random nucleation and subsequent growth. The kinetic analysis suggested that the accurate form of $g(\alpha)$ for combustion of the model soot investigated was $g(\alpha) = [-\ln(1-\alpha)]^{1/0.94}$. Hence, compared with an idealised Avrami–Erofeev equation, a non-integer value of kinetic exponent m was more appropriate to describe the actual combustion process.

Table 3
Values of the pre-exponential factors and kinetic exponents obtained for various heating rates

β (K min^{-1})	m	$\ln A$[a]
1.5	0.94	16.99
3.0	0.93	17.01
5.0	0.92	17.03
7.5	0.95	17.08
Mean values	0.94 ± 0.04	17.03 ± 0.12

[a] A in min^{-1}.

On the other hand, the comparison of E_a values derived by isoconversional and model-fitting methods were used to validate the chosen kinetic model. Hence, once the conversion model function was accurately determined by the master-plot method, the application of the Coats–Redfern (Eq. (8)) method resulted in activation energy and pre-exponential factor ($\ln A$) values (148 kJ mol^{-1} and 16.5, respectively) in relative good agreement with those derived by the composite kinetic method. It is therefore demonstrated that the model-fitting method is only useful (and relatively accurate) only when the reaction model is a priori known.

3.4. Thermo-kinetic curves reconstruction and stability prediction

Thermoanalytical curves were reconstructed to verify that the most accurate kinetic triplet (A, E_a, and model) was selected by the composite kinetic analysis method for each heating rate (Fig. 7). Hence, a relative good consistency was observed with respect to the actual thermoanalytical measurements, this pointing out that the composite kinetic analysis proposed was suitable for modelling the combustion processes under linear nonisothermal conditions. A certain deviation of theoretical values from experimental data was observed at the extremities of reaction (at both low and high α values). Hence, the oxidation of adsorbed hydrocarbons in the sample was markedly favoured in comparison with that of the solid matrix, and its presence could therefore influence the modelling of combustion process. Nevertheless, it was confirmed that the dominant reaction was successfully predicted. Likewise, the thermoanalytical curves were simulated by applying Eq. (8), which exclusively depends on the E_a value and the experimental data at a given heating rate. In this case, the data recorded at 1.5 K min^{-1} were used as reference data. A reasonable consistency was found among experimental data, model data obtained by using the full kinetic triplet (Eq. (1)), and model data generated through Eq. (8). Furthermore, the kinetic

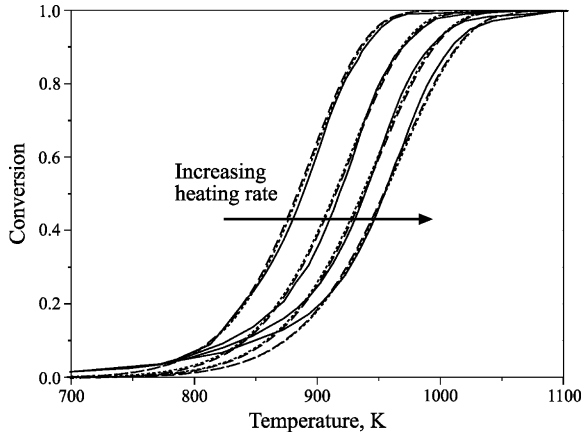

Fig. 7. Comparison between experimental (solid lines) and simulated thermoanalytical curves at a heating rate of 1.5, 3, 5 and 7.5 K min^{-1}. Dashed lines correspond to data obtained from Eq. (2), and dotted lines correspond to data obtained from Eq. (8).

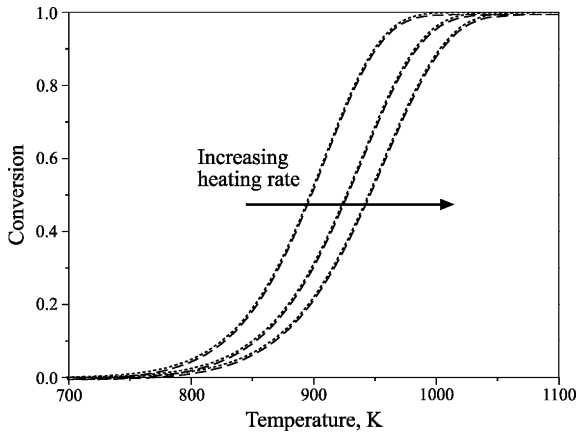

Fig. 8. Simulated thermoanalytical curves of the combustion of model soot at a heating rate of 2, 4 and 6 K min^{-1}. Dashed lines correspond to data obtained from Eq. (2), and dotted lines correspond to data obtained from Eq. (8).

triplet (Eq. (7)) was also used to predict the stability of the carbonaceous material at three different heating rates, namely 2, 4 and 6 K min^{-1} that were not used in the kinetic analysis (Fig. 8). For sake of comparison the simulation was also computed by Eq. (8) and experimental data at 1.5 K min^{-1} as well.

Also, isothermal simulations of the process were made. As in the case of nonisothermal analysis, reliable isothermal predictions could be carried out either using the full kinetic triplet or by means of Eq. (7), which requires a set of experimental data recorded at a given heating rate and the knowledge of E_a. Fig. 9 shows the isothermal behaviour of the material investigated at several specific temperatures deduced by both calculation techniques. The results were found to be in reasonable accordance in the 0–0.9 conversion range.

In summary, the reconstruction of kinetic curves and stability prediction could be performed depending upon the kinetic information available. It was demonstrated that the knowledge of E_a may be sufficient for a relatively accurate extrapolation of the kinetic behaviour. Obviously, if the full kinetic triplet were known, prediction of the reaction progress for required temperature profiles, and validation of the kinetic triplet would be assessed by simply computing Eqs. (1) and (2).

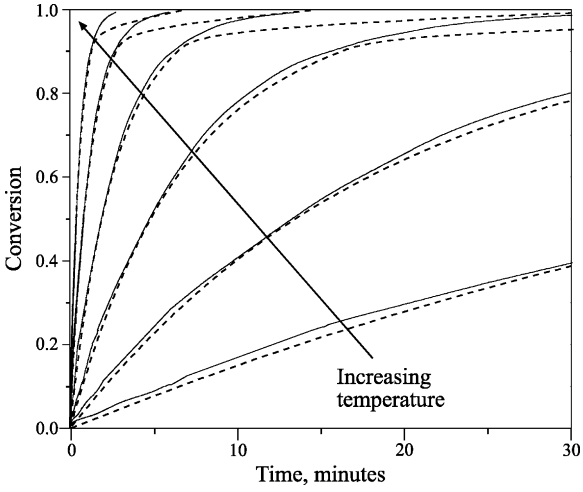

Fig. 9. Predictions of the isothermal decomposition of the model soot at several temperatures (923, 973, 1023, 1073, and 1123 K) calculated from Eq. (1) (solid lines) and Eq. (7) (dashed lines).

4. Conclusions

The kinetics of the heterogeneous combustion of synthetic soot was accurately determined from a series of thermoanalytical experiments at differing constant heating rates. The activation energy was calculated by the integral isoconversional KAS method without previous assumption regarding the conversion model fulfilled by the reaction. The activation energy was found to slightly depend on conversion, this suggesting that the combustion was a single-step process with an average activation energy of 153 kJ mol^{-1}. The master-plot method revealed that the conversion model $g(\alpha) = (-\ln(1-\alpha))^{1/m}$ ($m = 0.94$) best described the kinetics of the process. The formulation of such a relationship involved penetration of oxygen and subsequent combustion inside the porous structure. Changes in particle textural properties produced by the reaction were visualised ex situ by BET analysis of partially converted samples. The pre-exponential factor was calculated as well ($\ln A = 17.03$). Using the integral complete procedure above, it was possible to estimate satisfactorily the kinetic triplet of nonisothermal solid decomposition of the synthetic porous soot. As a result, an accurate simulation of the process was obtained. Likewise, estimated kinetic parameters allowed to predict the behaviour of the material under isothermal conditions.

To sum up it can be claimed that the proposed methodology for kinetic analysis allows for determining the kinetic parameters (the full kinetic triplet, conversion model and Arrhenius parameters) of the combustion process of model soot by means of relatively simple calculations techniques. Obtaining kinetic data simply requires thermoanalytical curves recorded at different heating rates. A strong point of this work is that the activation energy is calculated without assuming the conversion model or reaction order. This methodology can be applied to both commercial (synthetic) and real soot samples. As for real soot, which is characterised by the presence of a notable amount of adsorbed hydrocarbons, the proposed composite kinetic processing technique would eventually enable to separate and kinetically characterise the oxidation of adsorbed species and the combustion of the carbonaceous matrix. Note that this method is able to analyse the dependence of the activation energy with conversion. This of interest since usually the apparent activation energy values reported in the literature are related to the global process without a clear distinction between the combustion of the VOF and the solid. Finally, it is also noteworthy that this methodology can be used for evaluating the kinetics of other reactions involving the combustion of carbon such as the regeneration of catalysts deactivated by coking.

Acknowledgements

The authors wish to thank the Universidad del País Vasco/EHU (9/UPV 13517/2001) and the Ministerio de Edu-

ción y Ciencia (PPQ2002-037770 and CTQ2006-15079) for the financial support.

References

[1] C.D. Gamlin, N.K. Dutta, N.R. Choudhury, Polym. Degrad. Stabil. 80 (2003) 525–531.
[2] Y.K. Lee, D.J. Kim, H.J. Kim, T.S. Hwang, M. Rafailovich, J. Sokolov, J. Appl. Polym. Sci. 89 (2003) 2589–2596.
[3] M. Sorai, Comprehensive Handbook of Calorimetry and Thermal Analysis, John Wiley & Sons, Inc., Chichester, 2004.
[4] M.J. Starink, Thermochim. Acta 404 (2003) 163–176.
[5] W. Jiang, G. Nadeau, K. Zaghib, K. Kinoshita, Thermochim. Acta 351 (2000) 85–93.
[6] B. Dernaika, D. Uner, Appl. Catal. B 40 (2003) 219–229.
[7] M. Seipenbusch, J. Van Erven, T. Schalow, A.P. Weber, A.D. van Langeveld, J.C.M. Marijinissen, S.K. Friedlander, Appl. Catal. B 55 (2005) 31–37.
[8] J.H. Flynn, Thermochim. Acta 300 (1997) 83–92.
[9] A.W. Coats, J.P. Redfern, Nature 201 (1964) 68–69.
[10] M.E. Brown, M. Maciejewski, S. Vyazovkin, R. Nomen, J. Sempere, A. Burnham, J. Opfermann, R. Strey, H.L. Anderson, A. Kemmler, R. Keuleers, J. Janssens, H.O. Desseyn, C.R. Li, T.B. Tang, B. Roduit, J. Malek, T. Mitsuhashi, Thermochim. Acta 355 (2000) 125–143.
[11] B. Roduit, Thermochim. Acta 355 (2000) 171–180.
[12] P. Budrugeac, Polym. Degrad. Stabil. 74 (2001) 125–132.
[13] R. López-Fonseca, I. Landa, M.A. Gutiérrez-Ortiz, J.R. González-Velasco, J. Therm. Anal. Calorim. 80 (2005) 65–69.
[14] P. Simon, J. Therm. Anal. Calorim. 76 (2004) 123–132.
[15] H.E. Kissinger, Anal. Chem. 29 (1957) 1702–1706.
[16] J. Malek, Thermochim. Acta 200 (1992) 257–269.
[17] F.J. Gotor, J.M. Criado, J. Malek, M. Koga, J. Phys. Chem. A 104 (2000) 10777–10782.
[18] S. Vyazovkin, Int. J. Chem. Kinet. 28 (1996) 95–101.
[19] S.V. Vyazovkin, A.I. Lesnikovich, Thermochim. Acta 203 (1992) 177–185.
[20] G. Leofanti, M. Padovan, G. Tozzola, B. Venturelli, Catal. Today 41 (1999) 207–219.
[21] J.P.A. Neeft, F. Hoornaert, M. Makkee, J.A. Moulijn, Thermochim. Acta 287 (1996) 261–278.
[22] F. Bonnefoy, P. Gilot, B.R. Stanmore, G.A. Prado, Carbon 32 (1994) 1333–1340.
[23] B. Stanmore, P. Gilot, G. Prado, Thermochim. Acta 240 (1994) 79–89.
[24] F. Marcuccilli, P. Gilot, B. Stanmore, G. Prado, Proceedings of the 25th International Symposium International on Combustion, 1994, pp. 619–626.
[25] B.R. Stanmore, J.F. Brilhac, P. Gilot, Carbon 39 (2001) 2247–2268.
[26] A.K. Galwey, Thermochim. Acta 96 (1995) 259–273.
[27] P. Ciambelli, V. Vaccaro, S. Vaccaro, Catal. Today 17 (1993) 71–78.
[28] I.P. Kandylas, M. Stamatelos, Ind. Eng. Chem. Res. 38 (1999) 1866–1876.
[29] M.P. Bacos, J.L. Cochon, J.M. Dorvaux, O. Lavigne, Carbon 38 (2000) 93–103.
[30] R.H. Hurt, J.M. Calo, Combust. Flame 125 (2001) 1138–1149.
[31] G.A. Stratakis, A.M. Stamatelos, Combust. Flame 132 (2003) 157–169.
[32] H. Juang, D.B. Kittleson, M.R. Zachariah, Combust. Flame 136 (2004) 445–456.
[33] E. Cauda, D. Mescia, D. Fino, G. Saracco, V. Specchia, Ind. Eng. Chem. Res. 44 (2005) 9549–9555.
[34] G.A. Stratakis, Experimental investigation of catalytic soot oxidation and pressure drop characteristics in wall-flow diesel particulate filters, Ph.D. Thesis, University of Thessaly, Volos, Greece, 2004 and references therein. http://www.mie.uth.gr/labs/ltte/pubs/PhD_Stratakis.pdf.
[35] J. Opfermann, E. Kaisersberger, Thermochim. Acta 203 (1992) 167–175.
[36] J.P.A. Neeft, T.X. Nijhuis, E. Smakman, M. Makkee, J.A. Moulijn, Fuel 76 (1997) 1129–1136.
[37] M.N. Bokova, C. Decarne, E. Abi-Aad, A.N. Pryakhin, V.V. Lunin, A. Aboukaïs, Thermochim. Acta 428 (2005) 165–171.
[38] C. Di Blasi, F. Buonanno, C. Branca, Carbon 37 (1999) 1227–1238.
[39] Y.N.H. Nhon, H.M. Magan, C. Petit, Appl. Catal. B 49 (2004) 127–133.
[40] T. Ishiguro, N. Suzuk, Y. Fujitani, H. Morimoto, Combust. Flame 85 (1991) 1–6.